$(g-2)_{e,\mu}$ and strongly interacting dark matter with collider implications

Sarif Khan

ITP, George August University Goettingen

Talk at: ICHEP 2022, Bologna
Based on: JHEP07(2022)037 (2112.08393)
In Collaboration with: Anirban Biswas

July 07, 2022

SM Problems

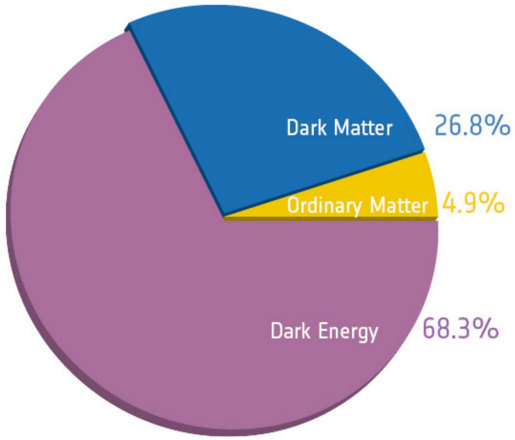

- We do not have any suitable particle candidate for dark matter in SM and its existence is confirmed from various observations.

SM Problems

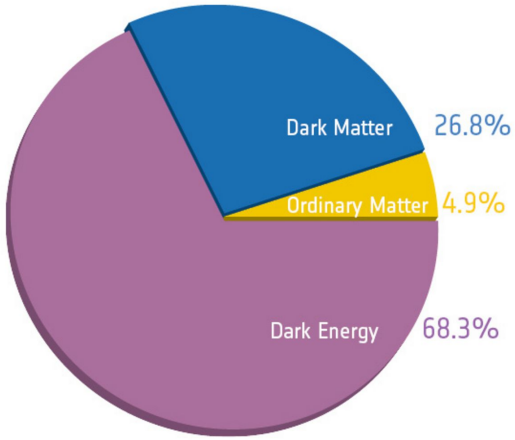

- We do not have any suitable particle candidate for dark matter in SM and its existence is confirmed from various observations.
- There exist matter anti-matter asymmetry of the Universe and we still finding its origin.

SM Problems

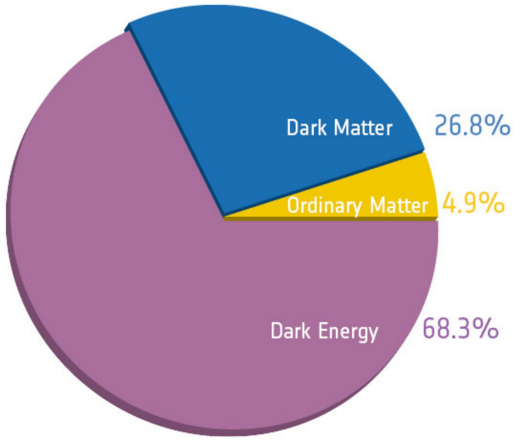

- We do not have any suitable particle candidate for dark matter in SM and its existence is confirmed from various observations.
- There exist matter anti-matter asymmetry of the Universe and we still finding its origin.
- In SM neutrinos are massless but oscillation experiments suggest they have mass.

SM Problems

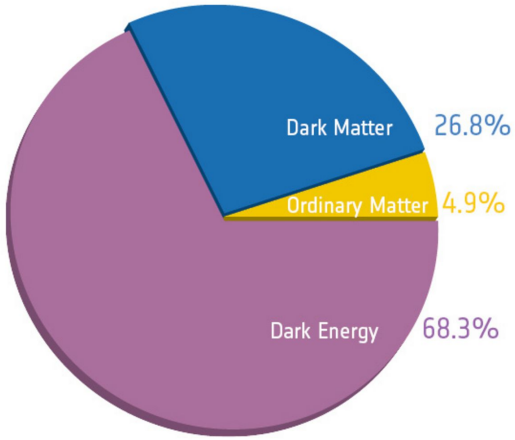

- We do not have any suitable particle candidate for dark matter in SM and its existence is confirmed from various observations.
- There exist matter anti-matter asymmetry of the Universe and we still finding its origin.
- In SM neutrinos are massless but oscillation experiments suggest they have mass.
- We also have a strong CP problem which deals with the the exact origin of the tininess of $\theta-$parameter.

Gauge group and Particle content

- We have considered $U(1)_{L_\mu - L_\tau}$ gauge extension of the SM.
- Particle content:

Gauge	Baryon Fields			Lepton Fields					Scalar Fields			
Group	$Q_L^i = (u_L^i, d_L^i)^T$	u_R^i	d_R^i	$L_L^i = (\nu_L^i, e_L^i)^T$	e_R^i	N_R^i	χ_L	χ_R	Φ_1'	Φ_2'	Φ_3'	Φ_4'
$\mathrm{SU(2)_L}$	2	1	1	2	1	1	1	1	2	2	1	1
$\mathrm{U(1)_Y}$	1/6	2/3	−1/3	−1/2	−1	0	−1	−1	1/2	1/2	0	0

Gauge	Baryonic Fields	Lepton Fields					Scalar Fields			
Group	(Q_L^i, u_R^i, d_R^i)	(L_L^e, e_R, N_R^e)	$(L_L^\mu, \mu_R, N_R^\mu)$	$(L_L^\tau, \tau_R, N_R^\tau)$	χ_L	χ_R	Φ_1'	Φ_2'	Φ_3'	Φ_4'
$\mathrm{U(1)}_{L_\mu - L_\tau}$	0	0	1	−1	1/3	1/3	0	−1/3	1	−1/3

Lagrangian

- Full Lagrangian for the above particles take the form:

$$\mathcal{L} = \mathcal{L}_{\rm SM} - \frac{1}{4}\hat{X}_{\alpha\beta}\hat{X}^{\alpha\beta} + \frac{\epsilon}{2}\hat{X}_{\alpha\beta}\hat{B}^{\alpha\beta} - g_{\mu\tau}\sum_{\substack{\ell=\mu,\nu_\mu,\\ \tau,\nu_\tau}} Q^{\ell}_{\mu\tau}\bar{\ell}\gamma^{\alpha}\ell\hat{X}_{\alpha} + \Big[i\,\bar{\chi}\partial\!\!\!/\chi - \bar{\chi}\gamma^{\alpha}\chi\left(\frac{g_{\mu\tau}}{3}\hat{X}_{\alpha} - g_1\hat{B}_{\alpha}\right)$$

$$-M_{\chi}\bar{\chi}\chi - \left(\beta^{R}_{e\chi}\overline{L_e}\Phi'_2\chi_R + \beta^{L}_{e\chi}\overline{e_R}\,\chi_L\Phi'_4 + h.c.\right)\Big] + \mathcal{L}_N + \sum_{i=2}^{4}\left(D_{\alpha}\Phi'_i\right)^{\dagger}\left(D^{\alpha}\Phi'_i\right) - \mathcal{V}(\Phi'_1,\Phi'_2,\Phi'_3,\Phi'_4)\,.$$

- Lagrangian associated with the right handed neutrinos,

$$\mathcal{L}_N = \frac{i}{2}\sum_{\substack{i=e,\mu,\\ \tau}}\overline{N_i}\partial\!\!\!/ N_i + \sum_{\substack{i=e,\mu,\\ \tau}}\left(y_{ii}\,\overline{L_i}\Phi'_1 N_i + h.c.\right) + \Big(M_{ee}N_eN_e + h_{e\mu}N_eN_\mu{\Phi'_3}^{\dagger}$$
$$+h_{e\tau}N_eN_\tau\Phi'_3 + M_{\mu\tau}e^{i\theta}N_\mu N_\tau + h.c.\Big)\,,$$

- DM interaction terms:

$$\mathcal{V}(\Phi'_1,\Phi'_2,\Phi'_3,\Phi'_4) = \sum_{i=2}^{4}\left[\mu_i^2\left({\Phi'}_i^{\dagger}\Phi'_i\right) + \lambda_i\left({\Phi'}_i^{\dagger}\Phi'_i\right)^2\right] + \sum_{i,j,j>i}\lambda_{ij}\left({\Phi'}_i^{\dagger}\Phi'_i\right)\left({\Phi'}_j^{\dagger}\Phi'_j\right)$$
$$+\lambda'_{12}\left({\Phi'}_1^{\dagger}\Phi'_2\right)\left({\Phi'}_2^{\dagger}\Phi'_1\right) + \left[\mu\left({\Phi'_1}^{\dagger}\Phi'_2\right){\Phi'_4}^{\dagger} + \xi\left(\Phi'_3{\Phi'_4}^{3}\right) + h.c.\right].$$

Muon and electron (g-2)

- Fermilab has announced a 4.2σ discrepancy between the experimental and theoretical value of $(g-2)_\mu$,

$$\Delta a_\mu = a_\mu^{\rm exp} - a_\mu^{\rm SM} = (2.51 \pm 0.59) \times 10^{-9}\,.$$

- Depending on the measurement of the fine structure constant, we have both negative and positive values for electron $(g-2)$,

$$\begin{aligned}
\Delta a_e &= a_e^{\rm exp} - a_e^{\rm B(LKB)} \\
&= (-8.8 \pm 3.6) \times 10^{-13} \text{ using } {}^{137}\text{Cs at Berkeley } (2.4\sigma)\,, \\
&= (+4.8 \pm 3.0) \times 10^{-13} \text{ using } {}^{87}\text{Rb at LKB } (1.6\sigma)
\end{aligned}$$

- We focus on negative value of electron $(g-2)$ and the positive value can also be explained very easily.

$(g-2)_{e,\mu}$ using abelian gauge boson

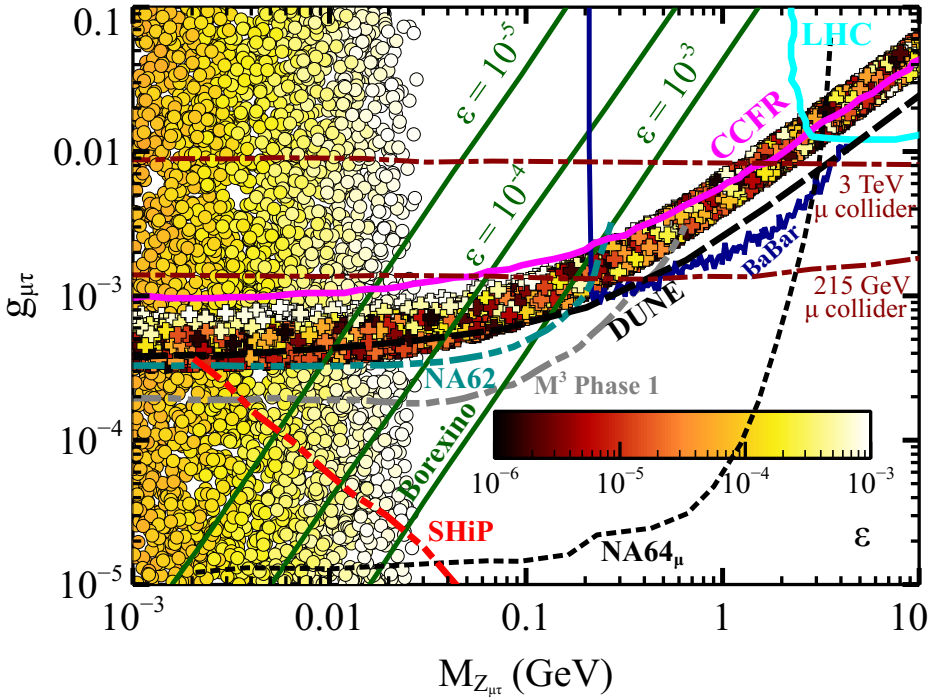

- Electron and muon $(g-2)$ can not be explained together.
- $g_{\mu\tau} - M_{Z_{\mu\tau}}$ plane will be accessed in future by the beam dump, accelerator neutrino experiments and rare kaon decays.
- We have taken into account the additional scalar contribution which will explain both the $(g-2)$ anomalies together.

Additional contribution to electron $(g-2)$

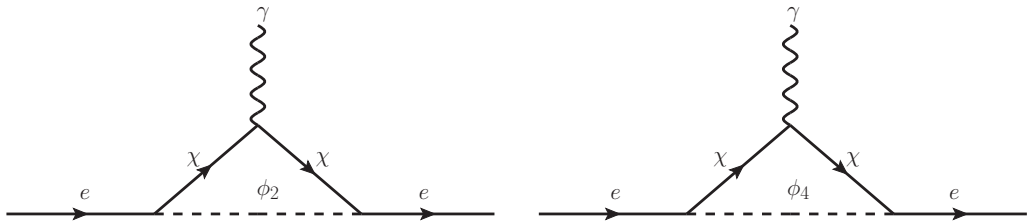

- The contributions to $(g-2)_e$ from the above diagrams takes the following form, **Leveille NPB 77**

$$\Delta a_e^{scalar} = -\frac{Q_{em}^{\chi}\, m_e}{8\pi^2}\left[(g_{\phi_2}^s)^2\,\mathcal{I}(m_e,\, M_\chi,\, M_{\phi_2}) + (g_{\phi_2}^p)^2\,\mathcal{I}(m_e,\, -M_\chi,\, M_{\phi_2})\right.$$
$$\left.(g_{\phi_4}^s)^2\,\mathcal{I}(m_e,\, M_\chi,\, M_{\phi_4}) + (g_{\phi_4}^p)^2\,\mathcal{I}(m_e,\, -M_\chi,\, M_{\phi_4})\right]\,,$$

where $\mathcal{I}(m_1, m_2, m_3)$ takes the following form,

$$\mathcal{I}(m_1,\, m_2,\, m_3) = \int_0^1 dx \frac{x^2 - x^3 + \frac{m_2}{m_1}x^2}{m_1^2 x^2 + (m_2^2 - m_1^2)x + m_3^2(1-x)}$$

SIMP DM diagrams

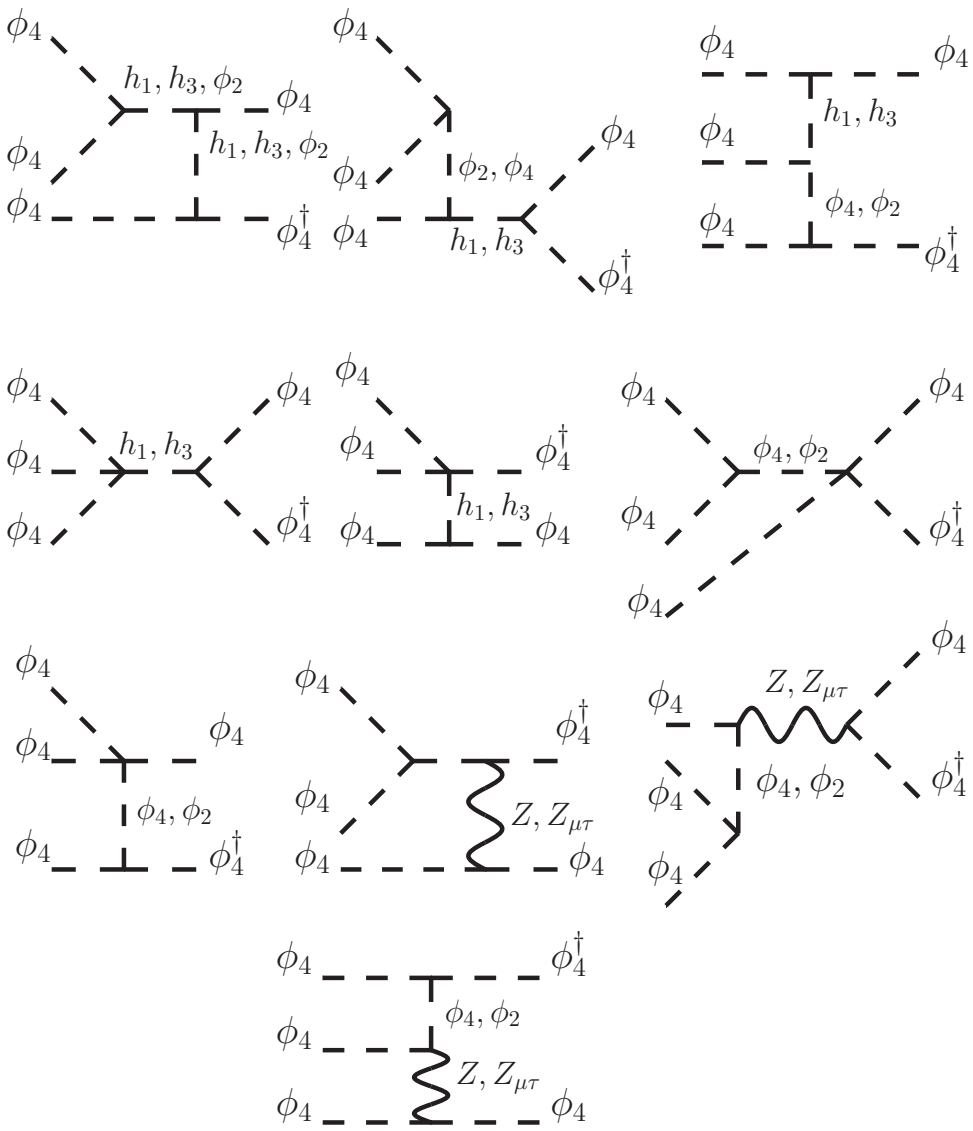

Bounds on SIMP DM

- **Self Interaction**: We have following self-interaction processes

$$\phi_4\phi_4 \to \phi_4\phi_4\,,\;\; \phi_4\phi_4^\dagger \to \phi_4\phi_4^\dagger\,,\;\; \phi_4^\dagger\phi_4^\dagger \to \phi_4^\dagger\phi_4^\dagger\,,$$

  and to be consistent with maximum number of observations from galaxies of DM self interaction, we have considered the limit $0.1\ \mathrm{cm}^2/\mathrm{g} \leq \frac{\sigma_{\mathrm{self}}}{M_{\phi_4}} \leq 10\ \mathrm{cm}^2/\mathrm{g}$.

- **Perturbativity and Unitarity:** We have considered perturbativity bound on the quartic couplings as $\lambda_i < 4\pi$ and unitarity of S-matrix demands $|\mathcal{M}| \leq 16\pi$.

- **Direct Detection bound:** The dark matter candidates ϕ_4 and $\phi_4^\dagger$ in the present model can be detected at the direct detection experiments by scattering with heavy nuclei and electrons as well. We have appropriately used the bounds on DM DD from different experiments.

Contd...

- **Kinetic equilibrium:** The kinetic equilibrium between the two sectors continues is primarily possible through elastic scatterings of dark matter with ν_μ and ν_τ where light gauge boson $Z_{\mu\tau}$ plays an important role.

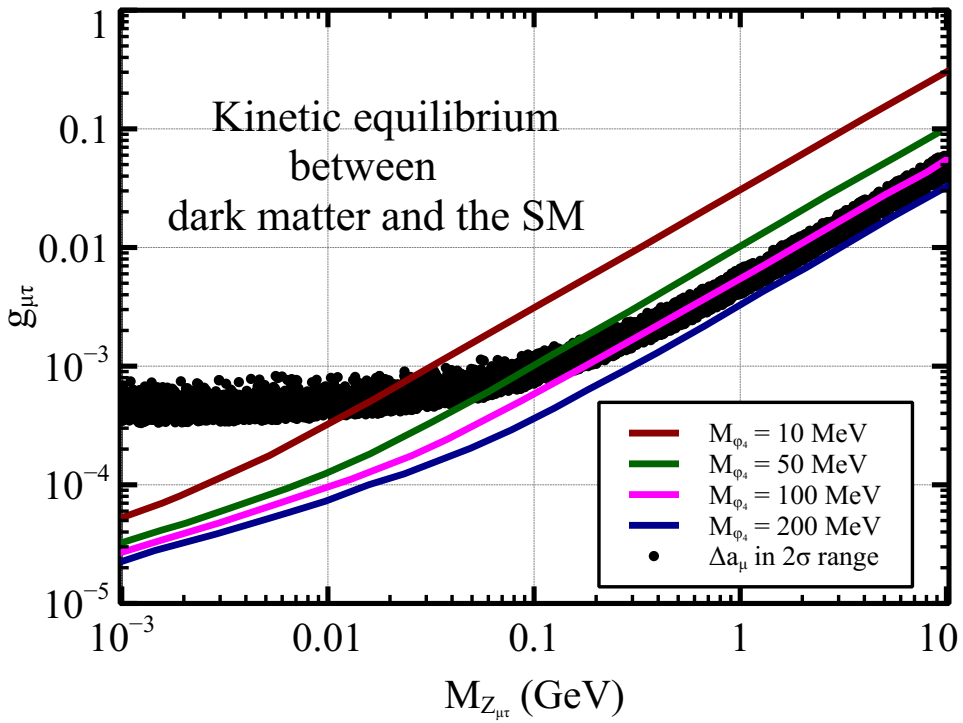

Contd...

- **Relic density bound:** The abundance of dark matter has been determined quite precisely by satellite borne CMB experiments particularly the Planck experiment and the current allowed range of dark matter relic density is [Planck' 18]

$$\Omega_{\rm DM} h^2 = 0.120 \pm 0.001$$

- **Invisible Higgs Decay:** SM like Higgs boson h_1 can decay into a pair of ϕ_4 and $\phi_4^\dagger$. Moreover, h_1 can decay into a pair of light gauge boson $Z_{\mu\tau}$ also. These additional decay modes contribute to the invisible decay of h_1. We consider total invisible decay of the Higgs boson [CMS' 18],

$$\mathrm{Br}(h_1 \to \text{invisible channels}) < 0.19\,.$$

SIMP DM Results: Line Plots

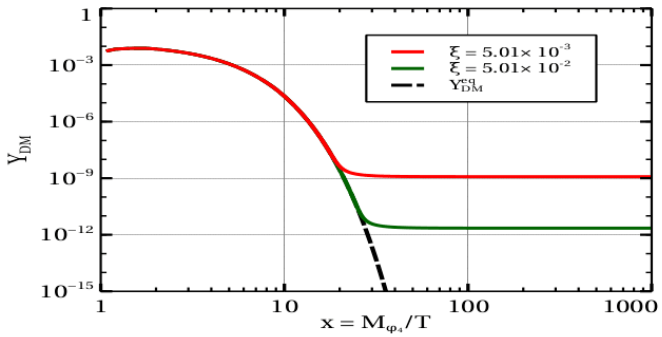

(a) $Y_{\rm DM}$ vs x plot for two different values of ξ

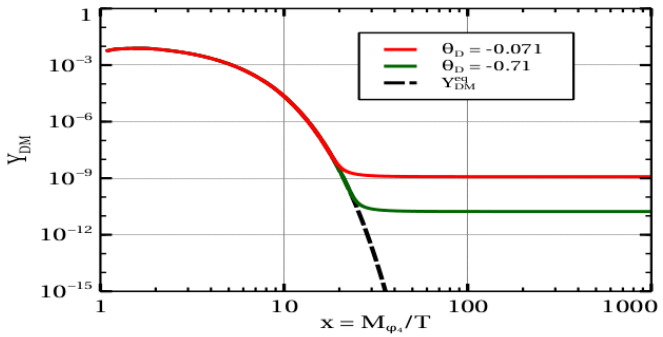

(b) $Y_{\rm DM}$ vs x plot for two different values of θ_D

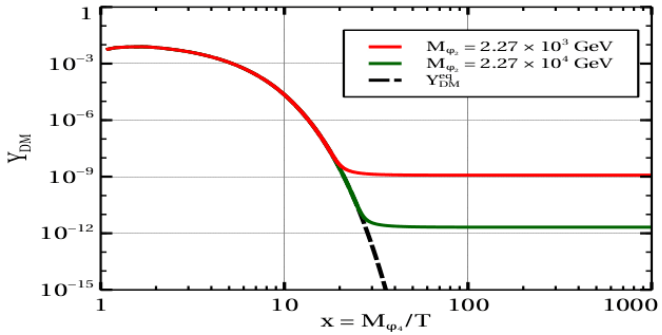

(c) $Y_{\rm DM}$ vs x plot for two different M_{ϕ_2}

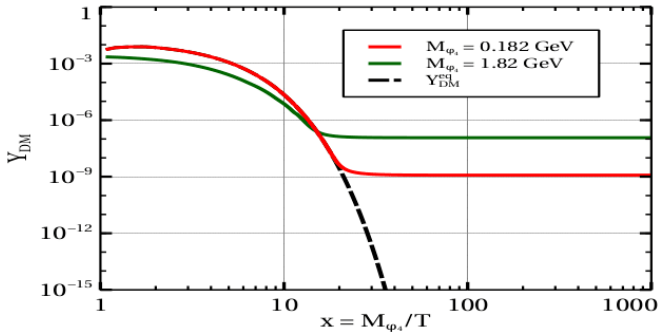

(d) $Y_{\rm DM}$ vs x plot for two values of M_{ϕ_4}

- Variation of DM relic density for different model parameters.

Contd...

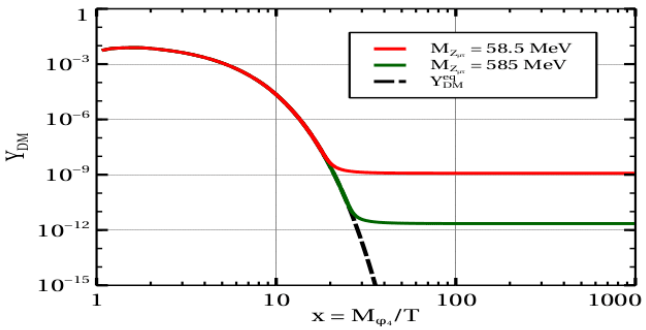

(e) $Y_{\rm DM}$ vs x plot for two values of $M_{Z_{\mu\tau}}$

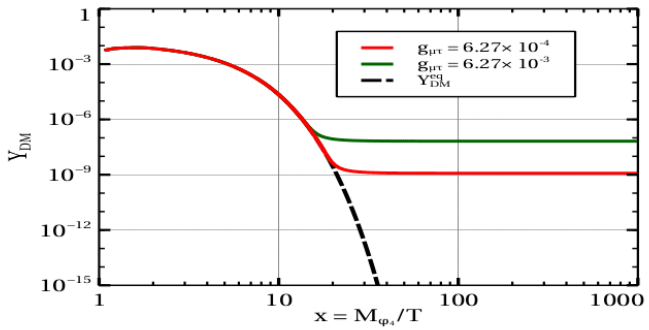

(f) $Y_{\rm DM}$ vs x plot for two different values of $g_{\mu\tau}$

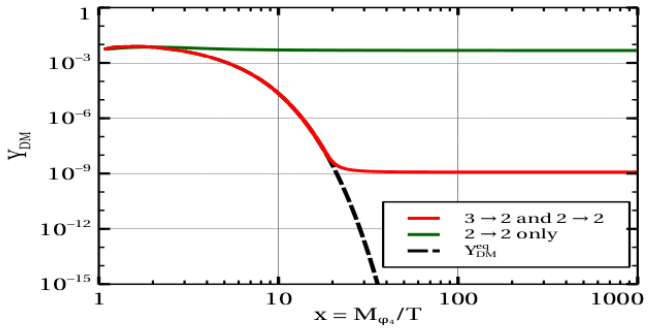

(g) Comparison on the effect of $3 \to 2$ and $2 \to 2$ scatterings in dark matter freeze-out

- Variation of DM relic density for another set of model parameters. Most importantly, $2 \to 2$ processes are subdominant compared to the $3 \to 2$ processes.

Scatter Plots

- We have varied the model parameters in the following range,

$$
\begin{aligned}
10^{-5} &\leq \xi \leq 1.0\,, \\
10^{-3}\ \text{rad} &\leq |\theta_D| \leq 0.1\ \text{rad}\,, \\
10^{-4} &\leq g_{\mu\tau} \leq 10^{-2}\,, \\
10^{-3}\ \text{GeV} &\leq M_{Z_{\mu\tau}} \leq 1.0\ \text{GeV}\,, \\
10^{3}\ \text{GeV} &\leq M_{\phi_4} \leq 10^{4}\ \text{GeV}\,, \\
10^{-2}\ \text{GeV} &\leq M_{\phi_2} \leq 10.0\ \text{GeV}\,,
\end{aligned}
$$

- Direct detection of DM,

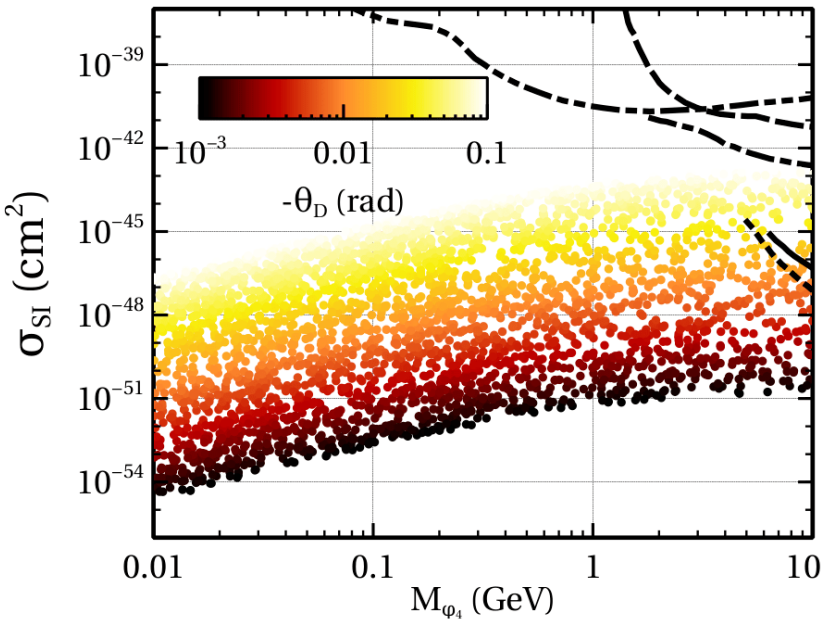

contd...

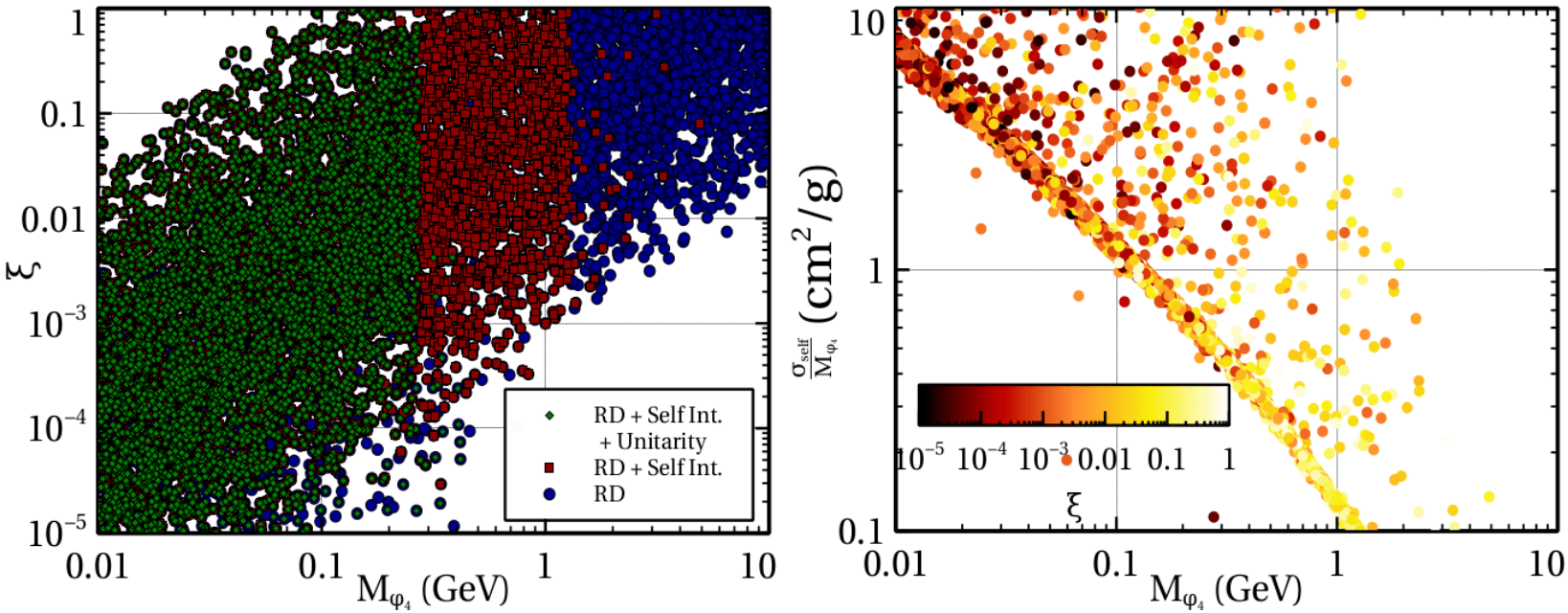

- LP shows the allowed region in $\xi - M_{\Phi_4}$ plane after applying different bounds.
- RP shows the variation of self interaction of DM with the DM mass.

Collider signature at e^+e^- collider

Production at collider

- Feynman diagrams for collider signature,

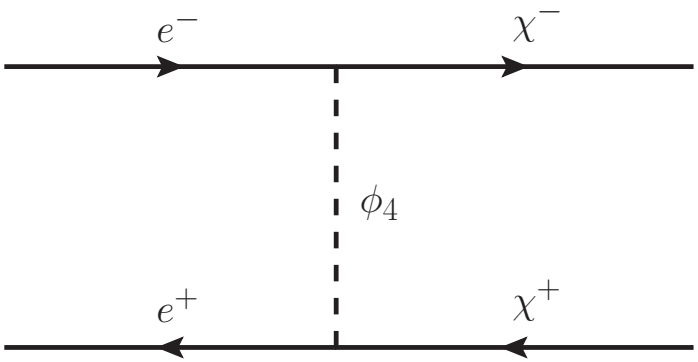

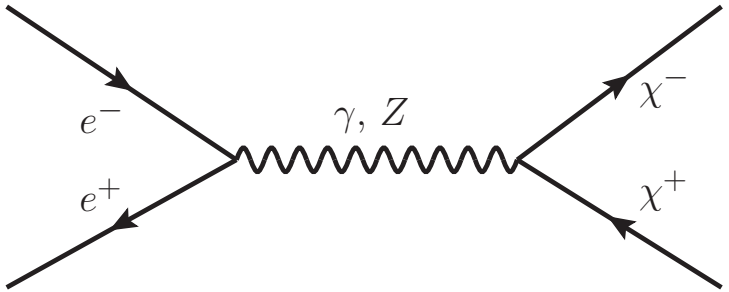

- Production CS at e^+e^- collider,

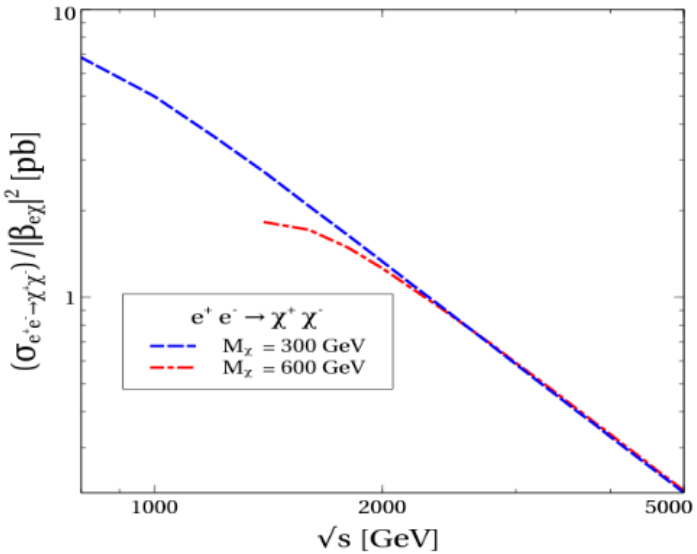

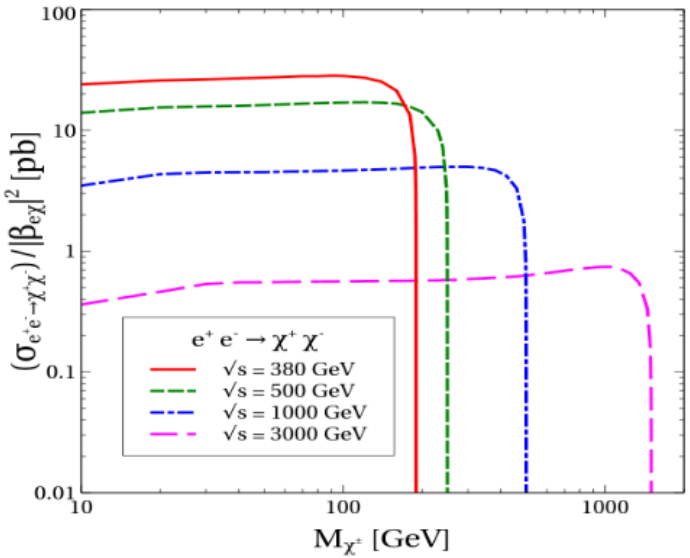

Histograms for signal and background

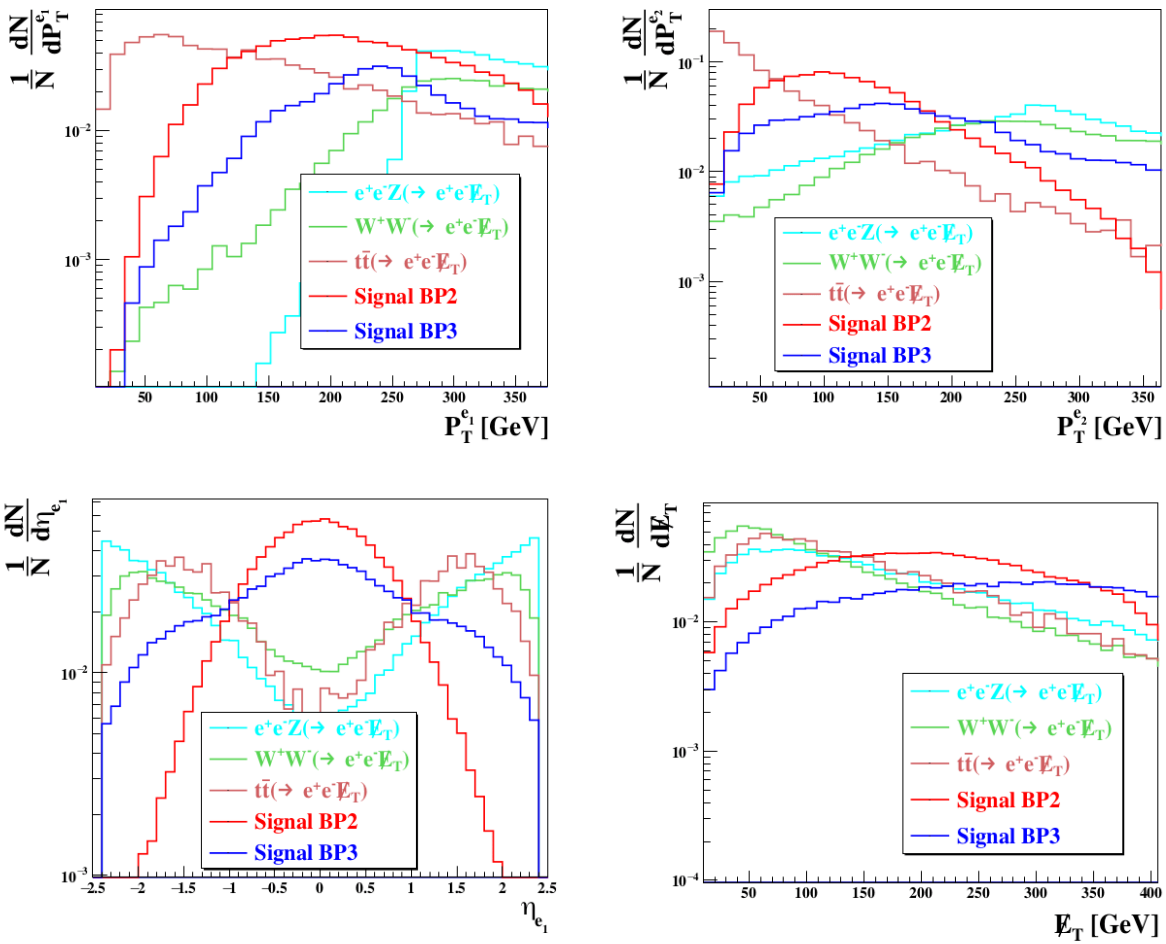

- We choose the suitable values for the kinematical variables to minimize the backgrounds.

SM BKGs after applying cuts

- SM BKGs at 1 TeV ILC after applying cuts,

SM Backgrounds at 1 TeV ILC		Effective Cross section after applying cuts (fb)					
Channels	Cross section (fb)	A0 + A1	A2	A3	A4	A5	A6
$e^+e^-Z\,(\to \nu_l\bar{\nu}_l)$	15.59	10.07	6.07	5.88	5.88	3.92	2.43
$W^+(\to e^+\nu_l)\,W^-(\to e^-\bar{\nu}_l)$	13.24	8.88	6.25	6.25	6.25	4.28	1.57
$t(\to be^+\nu_l)\,\bar{t}(\to \bar{b}e^-\bar{\nu}_l)$	1.61	0.73	0.20	0.20	0.05	0.04	0.02
Total Backgrounds							4.02

- SM BKGs at 3 TeV ILC after applying cuts,

SM Backgrounds at 3 TeV CLIC		Effective Cross section after applying cuts (fb)					
Channels	Cross section (fb)	A0 + A1	A2	A3	A4	A5	A6
$e^+e^-Z\,(\to \nu_l\bar{\nu}_l)$	6.18	2.95	2.85	2.83	2.83	1.06	0.82
$W^+(\to e^+\nu_l)\,W^-(\to e^-\bar{\nu}_l)$	1.44	0.74	0.73	0.73	0.73	0.36	0.27
$t(\to be^+\nu_l)\,\bar{t}(\to \bar{b}e^-\bar{\nu}_l)$	0.19	0.01	0.004	0.004	0.001	0.0006	0.0005
Total Backgrounds							1.09

Signal after applying different cuts

Signal at e^+e^- Collider				Effective CS after cuts (fb)						Stat Significance ($\mathcal{S}$)	
Experiment	Mass (GeV)	$\beta_{e\chi}$	CS (fb)	A0+A1	A2	A3	A4	A5	A6	$\mathcal{L} = 1$ fb^{-1}	$\mathcal{L} = 10$ fb^{-1}
1 TeV ILC	350.0	0.1	41.20	29.60	24.03	23.73	23.73	22.57	19.53	6.65	21.03
	450.0	0.1	29.56	21.30	19.83	19.60	19.60	19.50	17.38	6.11	19.32
3 TeV CLIC	600.0	0.1	5.13	2.91	2.78	2.78	2.78	2.16	2.05	1.60	5.04
	700.0	0.1	5.47	3.08	2.99	2.99	2.99	2.45	2.34	1.78	5.64

- The charged fermion with $e^+e^-\not{E}_T$ signal can be probed at the relatively early run of the ILC and CLIC collider.
- Charged fermion can be accessed at the 1 TeV collider more easily than the 3 TeV collider because of the smaller production at the 3 TeV collider.

$(g-2)_e$ and collider signature compatiability

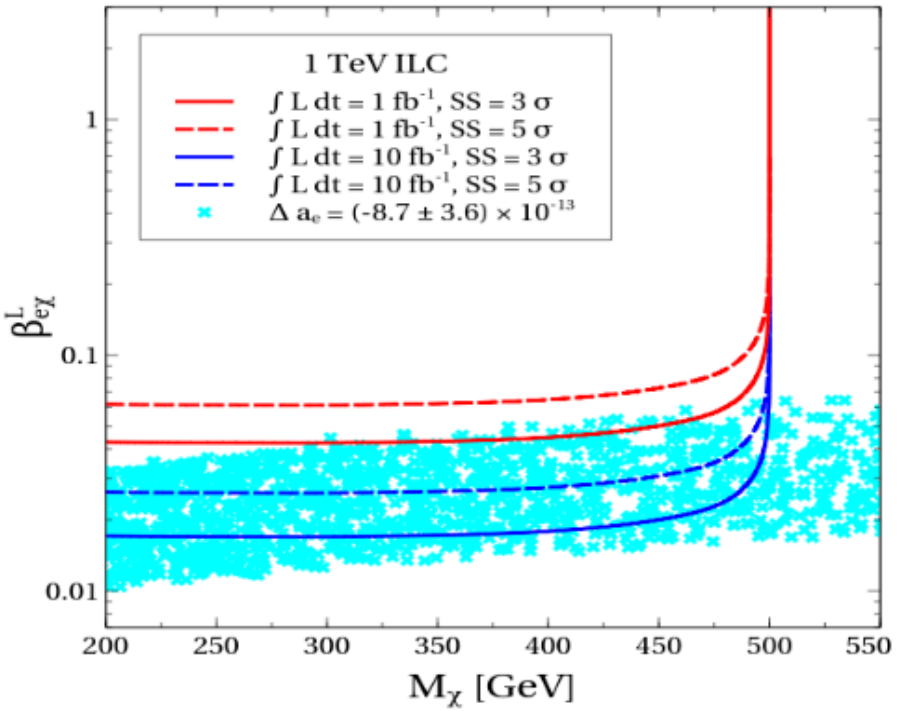

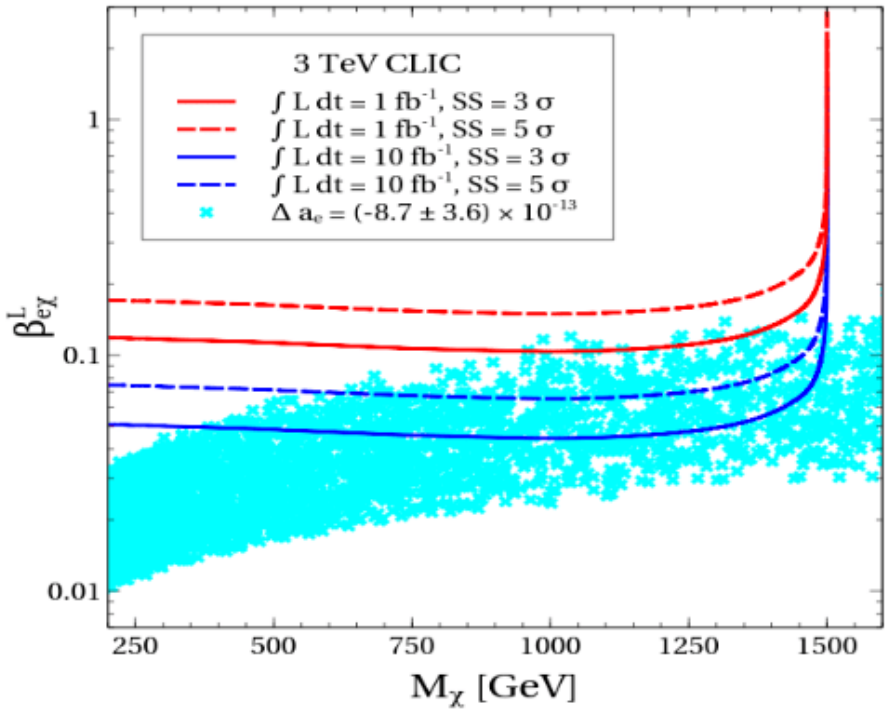

- Correct value of $(g-2)_{e,\mu}$ and the accessible region of the charged fermion at the e^+e^- collider have the overlapped region in $\beta^L_{e\chi} - M_\chi$ plane.

Overall Picture

Parameters/ Observables	BP1	BP2	BP3	BP4
M_{ϕ_4} (GeV)	29.216×10^{-3}	128.116×10^{-3}	168.756×10^{-3}	236.691×10^{-3}
M_{ϕ_2} (GeV)	7536.32	3511.42	1282.32	3123.67
$M_{Z_{\mu\tau}}$ (GeV)	39.405×10^{-3}	15.986×10^{-3}	124.048×10^{-3}	168.81×10^{-3}
$g_{Z_{\mu\tau}}$	6.626×10^{-4}	5.878×10^{-4}	1.003×10^{-3}	1.282×10^{-3}
$\theta_{\mu\tau}$	4.720×10^{-6}	4.720×10^{-6}	4.720×10^{-6}	4.720×10^{-6}
θ_D	-2.347×10^{-2}	-0.815×10^{-2}	-0.1422×10^{-2}	-9.559×10^{-2}
ξ	0.034×10^{-2}	1.022×10^{-2}	0.343×10^{-2}	0.413×10^{-2}
$\beta^L_{e\chi}$	0.12	0.22	0.70	0.066
$\beta^R_{e\chi}$	0.12	0.22	0.70	0.066
$\Omega_{\phi_4}h^2$	0.1191	0.1196	0.1199	0.1220
$\sigma_{\rm SI}$ (cm^2)	5.719×10^{-49}	1.317×10^{-49}	1.966×10^{-52}	6.958×10^{-45}
σ_{elec} (cm^2)	7.073×10^{-54}	1.057×10^{-55}	9.819×10^{-59}	1.994×10^{-51}
$\sigma_{\rm SD}$ (cm^2)	2.352×10^{-54}	5.416×10^{-55}	8.085×10^{-58}	2.861×10^{-50}
$\frac{\sigma_{\rm self}}{M_{\phi_4}}$ cm^2/g	3.171	1.024	0.808	0.529
Δa_μ	2.551×10^{-9}	2.995×10^{-9}	2.213×10^{-9}	2.502×10^{-9}
Δa_e	-9.867×10^{-13}	-9.620×10^{-13}	-9.441×10^{-13}	-9.661×10^{-13}

Conclusion

- The present model can accommodate neutrino mass with correct value of the oscillation parameters.
- We successfully explained $(g-2)_{e,\mu}$ together with the help of the scalar mediated one loop diagrams.
- Lightest among the scalars become a SIMP DM and we have addressed its detection prospects at different DM experiments.
- We have also explained collider analysis of charged fermion assisted by SIMP dark matter.
- The signal associated with the charged fermion can be probed at the early run of the e^+e^- collider.


Thank you

Backup

Cuts to minimize the background

A0. We have considered the events which contain opposite sign di-electron (e^+e^-) and transverse missing energy ($\not{E}_T$). We have also put the minimal cut on the transverse momentum of the electrons which is $p_{T,e}^{min} \geq 10$ GeV. We have collected the events which satisfy the pseudorapidity of the electrons $\eta_e < 2.5$. These cuts have been implemented at the time of the partonic generation of the events.

A1. We consider events that have opposite sign di-electron pair (e^+e^-) in the final state.

A2. From the left panel of Fig. (13), we can see that if we put strong cut on the leading electron $P_T^{e_1} \geq 130$ GeV then we can reduce the $t\bar{t}$ background. We have chosen relatively soft cut on the second leading electron which is $P_T^{e_2} \geq 60$ GeV .

A3. To reduce the background which comes from ZZ mode, we have used $Z-veto$. $Z-veto$ means, we have accepted the the events which violate the condition $|m_{ee} - 91.2| < 10$ GeV, where m_{ee} is the di-electron invariant mass.

A4. In order to eliminate the $t\bar{t}$ background, we have implemented $b-$veto. This implies we have rejected the events which contains $b-$quarks in the final state.

A5. From the left panel of Fig. (14), we can see that background and signal peak at different values of pseudorapidity. Therefore, to reduce the background without affecting the signal much we have considered the events which have pseudorapidity in the range, $|\eta^e| < 1.5$.

A6. From the right panel of Fig. (14), we can see that if we implement a cut on the transverse missing energy then background can be reduced significantly. We have adapted the missing energy cut which is $\not{E}_T > 160$ GeV.